Possible increased frequency of ENSO-related dry and wet conditions over some major watersheds in a warming climate

Qiaohong Sun, Chiyuan Miao, Amir AghaKouchak, Iman Mallakpour, Duoying Ji, and Qingyun Duan

2020

Original citation:
Sun, Q., Miao, C., AghaKouchak, A., Mallakpour, I., Ji, D., & Duan, Q. (2020). Possible increased frequency of ENSO-related dry and wet conditions over some major watersheds in a warming climate. *Bulletin of the American Meteorological Society*, *101*(4), E409-E426. https://doi.org/10.1175/BAMS-D-18-0258.1

BAMS Article

Possible Increased Frequency of ENSO-Related Dry and Wet Conditions over Some Major Watersheds in a Warming Climate

Qiaohong Sun, Chiyuan Miao, Amir AghaKouchak, Iman Mallakpour, Duoying Ji, and Qingyun Duan

ABSTRACT: Predicting the changes in teleconnection patterns and related hydroclimate extremes can provide vital information necessary to adapt to the effects of the El Niño–Southern Oscillation (ENSO). This study uses the outputs of global climate models to assess the changes in ENSO-related dry/wet patterns and the frequency of severe dry/wet events. The results show anomalous precipitation responding asymmetrically to La Niña and El Niño, indicating the teleconnections may not simply be strengthened. A "dry to drier, wet to wetter" annual anomalous precipitation pattern was projected during La Niña phases in some regions, with drier conditions over southern North America, southern South America, and southern central Asia, and wetter conditions in Southeast Asia and Australia. These results are robust, with agreement from the 26 models and from a subset of 8 models selected for their good performance in capturing observed patterns. However, we did not observe a similar strengthening of anomalous precipitation during future El Niño phases, for which the uncertainties in the projected influences are large. Under the RCP4.5 emissions scenario, 45 river basins under El Niño conditions and 39 river basins under La Niña conditions were predicted to experience an increase in the frequency of severe dry events; similarly, 59 river basins under El Niño conditions and 61 river basins under La Niña conditions were predicted to have an increase in the frequency of severe wet events, suggesting a likely increase in the risk of floods. Our results highlight the implications of changes in ENSO patterns for natural hazards, disaster management, and engineering infrastructure.

https://doi.org/10.1175/BAMS-D-18-0258.1
Corresponding author: Chiyuan Miao, miaocy@vip.sina.com
Supplemental material: https://doi.org/10.1175/BAMS-D-18-0258.2
In final form 5 November 2019

AFFILIATIONS: Sun—State Key Laboratory of Earth Surface Processes and Resource Ecology, Faculty of Geographical Science, Beijing Normal University, Beijing, China, and Center for Hydrometeorology and Remote Sensing, Department of Civil and Environmental Engineering, University of California, Irvine, Irvine, California; **Miao and Duan**—State Key Laboratory of Earth Surface Processes and Resource Ecology, Faculty of Geographical Science, Beijing Normal University, Beijing, China; **AghaKouchak and Mallakpour**—Center for Hydrometeorology and Remote Sensing, Department of Civil and Environmental Engineering, University of California, Irvine, Irvine, California; **Ji**—College of Global Change and Earth System Science, Beijing Normal University, Beijing, China

Climate models project a general increase in the frequency and intensity of hydroclimate extremes at regional to global spatial scales during the twenty-first century (Donat et al. 2017; Hirabayashi et al. 2013), which is expected to cause severe casualties and economic loss (Ward et al. 2014). This enhancement of extreme events is due to increases in atmospheric water vapor and rates of ascent in clouds (O'Gorman and Schneider 2009; Pfahl et al. 2017). Along with these climatic changes, the Earth system continues to experience natural interannual climate variability. The El Niño–Southern Oscillation (ENSO) is a naturally occurring fluctuation that originates in the tropical Pacific region and dominates global interannual climate variability by modulating large-scale atmospheric circulation patterns (Neelin et al. 1998; Alexander et al. 2002). ENSO affects the occurrence of many natural hazards (e.g., droughts, floods, hurricanes) (Ward et al. 2014; Sun et al. 2016) and modulates the societal risks arising from these hazards (e.g., wildfires, disruption of food production, death toll) (Andela and Werf 2014; Iizumi et al. 2014; Power and Callaghan 2016) in many regions of the world. Kenyon and Hegerl (2008, 2010) investigated the global response patterns of hydroclimate extremes to ENSO over land areas, and reported a significant decrease in precipitation extremes over Southeast Asia, Indonesia, Australia, and the northernmost region of South America during El Niño phases, whereas the southern tier of the United States and the region from Argentina to southern Brazil show increases in heavy precipitation during El Niño phases, and vice versa during La Niña phases (Kenyon and Hegerl 2010). Many record-breaking drought and flood events can be linked directly to the ENSO cycle, such as the November–April 1998–2001 severe drought in southwest Asia, which was linked to the cold phase of the ENSO cycle (Barlow et al. 2002; Hoerling and Kumar 2003), extreme floods in China and Australia (Yin and Li 2001) and Bangladesh (Hoerling and Kumar 2003; Bell et al. 1999) in 1998, and the severe heat and drought in Indonesia in 2015 (King et al. 2016).

Global warming changes the climate state in tropical Pacific regions (Allen and Luptowitz 2017; Wang et al. 2016), leading to changes in the characteristics of ENSO, and it might have already increased the likelihood of extreme events (Cai et al. 2014, 2015a,b; Power et al. 2017). Changes in the mean state of tropical Pacific regions and in the properties and features of ENSO may alter ENSO teleconnections, precipitation variability, and the occurrence of droughts and floods over remote land areas. ENSO-driven precipitation variability in the equatorial Pacific is projected to intensify in response to global warming, and this tends to increase ENSO-driven precipitation variability around the world (Bonfils et al. 2015; Power and Delage 2018). In addition, El Niño–driven precipitation anomalies in the equatorial Pacific are projected to move east (e.g., Kug et al. 2010; Power et al. 2013), inducing an eastward shift in the Pacific–North American (PNA) teleconnection pattern (Zhou et al. 2014; Kug et al.

2010). Intensification of El Niño–driven drying in the western Pacific Ocean is also predicted under global warming (Power et al. 2013). For Central America, the projected future changes in precipitation anomalies are not clear (Steinhoff et al. 2015). Tropical cyclones are predicted to become more frequent during future El Niño events compared with present El Niño events (Chand et al. 2017). Studies have also suggested that the teleconnection mechanisms that underlie ENSO and its associated impact on North America will intensify and/or shift position as a result of climate anomalies in a warmer climate (Coelho and Goddard 2009; Wang et al. 2014; Wang et al. 2015; Meehl et al. 2007). The projected increases in both intense drought and excessive flooding in California may be associated with a strengthened relation to ENSO, which affects the hydrologic cycle through its precursor patterns as well as through its warm and cold phases (Yoon et al. 2015).

Some recent studies examined changes in ENSO-driven precipitation variability over global land in the twenty-first century (Power and Delage 2018; Bonfils et al. 2015; Perry et al. 2017). Perry et al. (2017) reported a ~12% increase in the spatial extent of ENSO teleconnections for precipitation. Power and Delage (2018) reported an increase in ENSO-related variability over some regions, driven by the enhanced variability in the tropical Pacific. Yeh et al. (2018) reviewed changes in ENSO atmospheric teleconnections associated with changes in ENSO properties and the tropical Pacific mean state, and how these may change under greenhouse warming. Here, we extend these previous studies as follows: 1) we use global climate models to estimate future changes in ENSO-related precipitation teleconnection patterns at both the local grid scale and the river-basin scale, and 2) we quantify changes in the frequency of ENSO-related extreme precipitation events in major river basins worldwide. We use simulations from 26 models from phase 5 of the Coupled Model Intercomparison Project (CMIP5), statistically downscaled via the bias correction and spatial downscaling method (BCSD; Brekke et al. 2014). In these simulations, climate projections are downscaled to obtain high spatial resolution and to reduce climatological bias (Maurer et al. 2014). Using these models, we calculate a global projection of the changes in ENSO-related hydroclimate extremes over land under the representative concentration pathway (RCP) 4.5 emissions scenario for the twenty-first century.

Materials and methods

Observed data. In this study, a gridded monthly precipitation product for the period 1951–2005 from the Global Precipitation Climatology Centre (GPCC) with a grid resolution of 0.5° was used to calculate the standardized precipitation index (SPI). The SPI is a widely used index for characterizing dry/wet events. We used the 3-month-scale SPI to identify dry/wet conditions, since the 3-month SPI reflects short- and medium-term moisture conditions and provides a seasonal estimation of precipitation. The 3-month SPI compares the precipitation for a given 3-month period over the historical record. For example, a 3-month SPI value for the end of February compares the precipitation total for the December–February period with all the past totals for that same period. This long-term record is fitted to a probability distribution, which is then transformed into a normal distribution such that the mean SPI value for the location and desired period is zero. Positive SPI values indicate greater than median precipitation, and negative values indicate less than median precipitation. Because the SPI is normalized and dimensionless, it is particularly suited for characterizing the relative dry/wet conditions across different time periods and across regions with different climatic conditions and seasons. To reduce the influence of dry month and location, we calculated the running 3-month total precipitation, and screened out the months/locations with a long term average of the 3-month total precipitation below 30 mm.

We used the oceanic Niño index (ONI; 3-month running mean of ERSST.v4 SST anomalies in the Niño-3.4 region) to represent ENSO and determine whether El Niño or La Niña

conditions were present. The ONI series is calculated from centered 30-year base periods updated every 5 years. Updating the base periods removes the overall warming trend and therefore more accurately reflects interannual ENSO variability. For instance, ONI values for the period 1950–55 are based on the 1936–65 base period, ONI values for the period 1956–60 are based on the 1941–70 base period, and so on. More details can be found at https://origin.cpc.ncep.noaa.gov/products/analysis_monitoring/ensostuff/ONI_change.shtml.

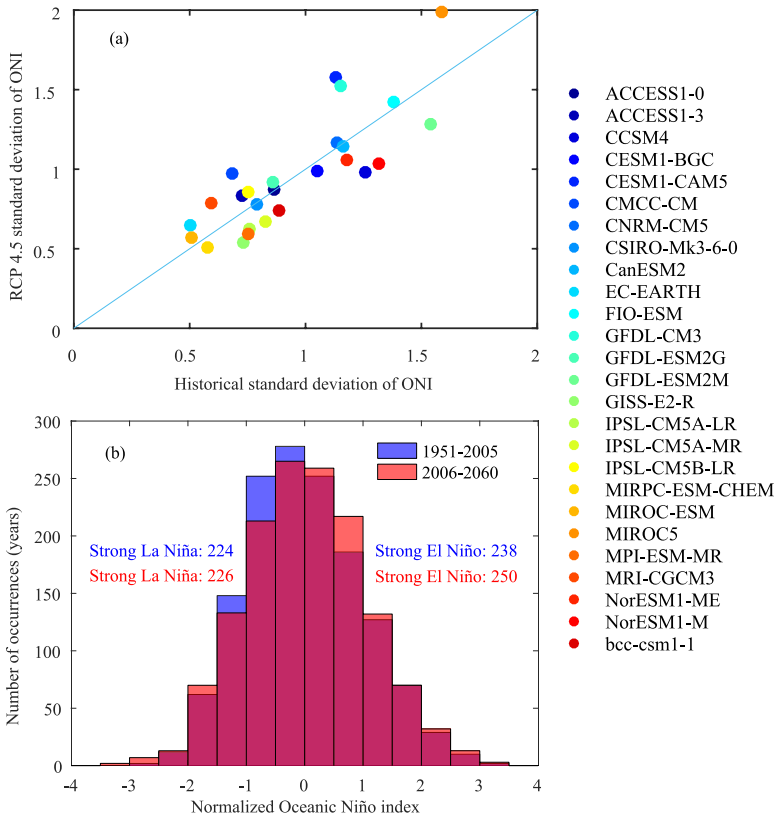

FIG. 1. (a) Standard deviation of the ONI and (b) the total number of strong La Niña and El Niño years generated by 26 models for the historical (1951–2005) and RCP4.5 (2006–60) simulations.

CMIP5 model output. We quantified dry/wet conditions in the simulated data by calculating the SPI based on BCSD precipitation simulations from 26 CMIP5 Earth system models (0.5° × 0.5° grid resolution) (see Table ES1 in the online supplement). BCSD is one of the most widely used statistical downscaling methods and is used to generate temperature and precipitation datasets with higher spatial resolution and significantly reduced climatological biases (Wood et al. 2004). The BCSD CMIP5 simulations have been used to project future changes in climate extremes in previous studies (Ning et al. 2015). In this study, each simulation spanned the years 1951–2060. For 1951–2005, we used estimates of historical climate forcings. For 2006 onward, we used forcings corresponding to RCP4.5, which represents a relatively moderate buildup of atmospheric greenhouse gases. For each model, we then used the BCSD precipitation output to calculate the 3-month SPI time series.

Classification of El Niño, neutral, and La Niña years. Related atmospheric and rainfall variability can be strongly associated with different stages of ENSO events. We used the standard hydrological year (October–September) to calculate the time series of the annual SPI value, as previous studies have done (Ward et al. 2014). ENSO years were therefore adjusted by 1 year to be connected with the hydrological year. For instance, ENSO year 1998 refers to the period October 1998 to September 1999. The ONI for December–February (DJF), when ENSO events are typically at their peak (Santoso et al. 2013), was used as ENSO index to classify years as neutral years ($-0.5\sigma < \text{ONI} < 0.5\sigma$), normal La Niña years ($-1.0\sigma < \text{ONI} < -0.5\sigma$), strong La Niña years ($\text{ONI} < -1.0\sigma$), normal El Niño years ($0.5\sigma < \text{ONI} < 1.0\sigma$), or strong El Niño years ($\text{ONI} > 1.0\sigma$), where σ is the standard deviation of the ONI. The ONI calculation was applied to the Niño-3.4 time series from each of the 26 models. Compared with the standard deviation of historical ONI time series, 14 models had higher ONI variability in the projected simulation (2006–60) (Fig. 1a). We used the standard deviation of the ONI during the period 1951–2005 to normalize the ONI in both the historical and RCP4.5 simulations.

In this study, we focused on the influence of the strong El Niño and La Niña events. Using the threshold value of 1.0σ, 226 strong La Niña and 250 strong El Niño events were selected from the 26 models in the projected period (2006–60, Table ES2); these numbers

were slightly higher than the numbers in the historical period (Fig. 1). Raising the threshold value to 2.0σ yielded 17.07% and 64.29% increases in the frequency of strong El Niño and strong La Niña events. These changes mainly arise from a small number of models and are not robust. Previous studies taking into account the nonlinear nature of ENSO processes also predicted that the frequency of extreme ENSO events will increase (Cai et al. 2014, 2015a,b; Power et al. 2017).

ENSO-related precipitation responses

Precipitation response pattern. A composite analysis was performed to investigate precipitation response patterns to La Niña, El Niño, and neutral years. We first selected the strong La Niña, strong El Niño, and neutral years based on the ONI values in the observations and in each model. Then, we detrended the annual SPI time series during the period 1951–2060 for all model simulations. We computed the detrended annual SPI average for each grid location over all of the strong La Niña and strong El Niño years during the 1951–2005 and 2006–60 periods to obtain composite patterns for each set of events. The Mann–Whitney *U* test was used to determine whether the composite patterns for strong La Niña and strong El Niño years were statistically significantly different from the composite pattern for neutral years. The Mann–Whitney *U* test is a nonparametric test and does not require the assumption of normality. Then, we compared the composite patterns for the 1951–2005 and the 2006–60 periods to identify changes in ENSO-related precipitation variability between the two periods. We focused on the grid cells where the signals were strong for the present day in both the model and the observations. We first selected the grid cells over global land that had a significant ($p < 0.1$) correlation between the time series of the annual detrended SPI and the ENSO index (observations) during the period 1951–2005. Then, we assessed the correlation relationship between the time series of the annual detrended SPI and ENSO index during the period 1951–2005 over these grid cells in all models. We selected the grid cells where the multimodel ensemble mean (MMM) of all 26 models correctly captured the observed signal of the correlation relationship and where more than two-thirds of the models (i.e., 17 models) agreed with the observed signals. The geographical distribution of the grid cells to be analyzed can be found in Fig. ES1 in the online supplement (https://doi.org/10.1175/BAMS-D-18-0258.2).

We also examined changes in the patterns of precipitation at the river-basin scale. River-basin boundaries were based on the Global Runoff Data Centre (GRDC) dataset. This dataset contains a basin layer for 405 river basins. We selected 167 river basins over global land that had a significant ($p < 0.1$) correlation between the time series of the regional average annual detrended SPI and the ENSO index (observations) during the period 1951–2005. Then, we chose the river basins where the MMM correctly captured the observed signals and where more than two-thirds of the models agreed with those signals. In the end, 117 river basins were selected (Fig. ES1b). Regional SPI composites for these 117 river basins during the strong La Niña and strong El Niño years were calculated for the observations and for all models for the 1951–2005 and 2006–60 periods to compare the changes in regional precipitation variability forced by the future ENSO events.

In addition to analyzing the MMM of all 26 models, we also wanted to take the capabilities of the different models into consideration; therefore, we also compared the results with those of a subset of models that showed good performance in relation to the observations. Because our study mainly focused on the influence of ENSO on dry/wet conditions over global land, we selected the models that reasonably captured the observed SPI response pattern to La Niña and El Niño phases at both the local gridcell scale and the river-basin scale. First, we selected the 10 models with the highest spatial correlation coefficients (the Pearson correlation coefficient between the SPI values taken over all selected cells from the model and observed

composite patterns) between observed and simulated data (Fig. 2). Following the methods in Cai et al. (2014), we used Niño-3.4 SST skewness (Table ES3) as an additional selection criterion because we used the ONI to identify ENSO events. The skewness of the Niño-3.4 SST anomaly coarsely measures asymmetry in the El Niño–La Niña amplitudes. Eight out of the 26 total CMIP5 models had both positively skewed Niño-3.4 SST (like the observed data) and high correlations with the observed SPI response pattern (Fig. 2). The eight models that met our criteria are the ACCESS1.3, CCSM4, CESM1(BGC), CNRM-CM5, GFDL CM3, GFDL-ESM2G, GFDL-ESM2M, and NorESM1-ME. The majority of these selected models coincide with those used by Cai et al. (2014).

Frequency of severe dry/wet events. To investigate potential changes in the occurrence of ENSO-related extreme precipitation events, we calculated the difference in the frequency of severe dry/wet events between the historical and projected periods (Table ES4) over global land and over major river basins (the 117 selected river basins are shown in Fig. ES1). The SPI time series was detrended for each month during the period 1951–2060. For the strong La Niña and strong El Niño years, we accumulated the number of months per year in which the detrended SPI values exceeded 1.5 (severe wet) or –1.5 (severe dry) over global land (grid scale) or at the river-basin scale. For instance, for a river basin covering N grid cells, a severe dry event means that at least one of these grid cells experienced one severe dry month in the year; the "severe dry event" value for this river basin can take values ranging from 0 to 12 × N. We averaged the number of severe dry and wet events occurring in strong La Niña years and in strong El Niño years, and then estimated the relative and absolute change in the average number of severe dry/wet events during the projected period.

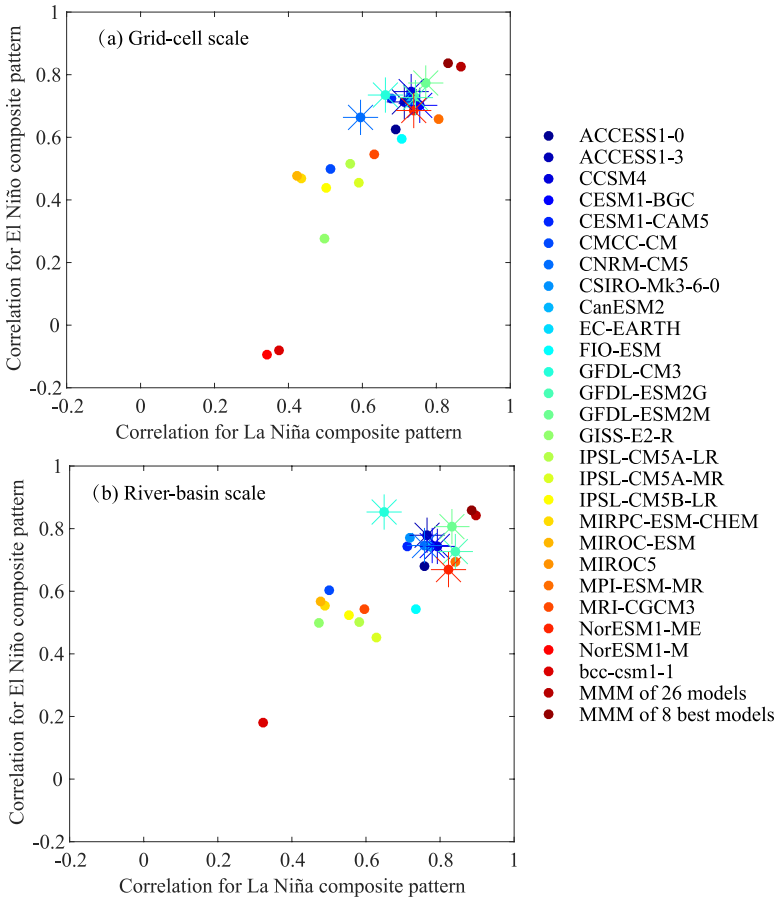

Fig. 2. Spatial correlation coefficients for the relationship between observed and simulated regional SPI composite values at (a) the gridcell scale and (b) the river-basin scale. The grid cells and river basins where the ensemble mean captured the observed signal of the correlation relationship and where more than two-thirds of the models agreed with the observed and MMM signals are included in the analysis. Results are shown for 26 individual CMIP5 models plus the MMMs. The asterisk dots indicate the 8 models out of the 26 total models that had both positively skewed Niño-3.4 SST (like the observed data) and higher correlations than the other models.

Results

Comparison with the observed precipitation response pattern to ENSO. Figure ES2 showed the observed correlation relationship between the ENSO and the SPI values during the period 1951–2005. Figures ES3a and ES4a showed the observed dry/wet patterns in response to both La Niña and El Niño phases. The anomalous precipitation patterns in response to ENSO were generally consistent with those reported in previous studies (Barlow et al. 2002; Grimm and Tedeschi 2009; Mariotti 2007; Juneng and Tangang 2005; Ropelewski and Halpert 1986, 1987; Richard et al. 2000), with drier

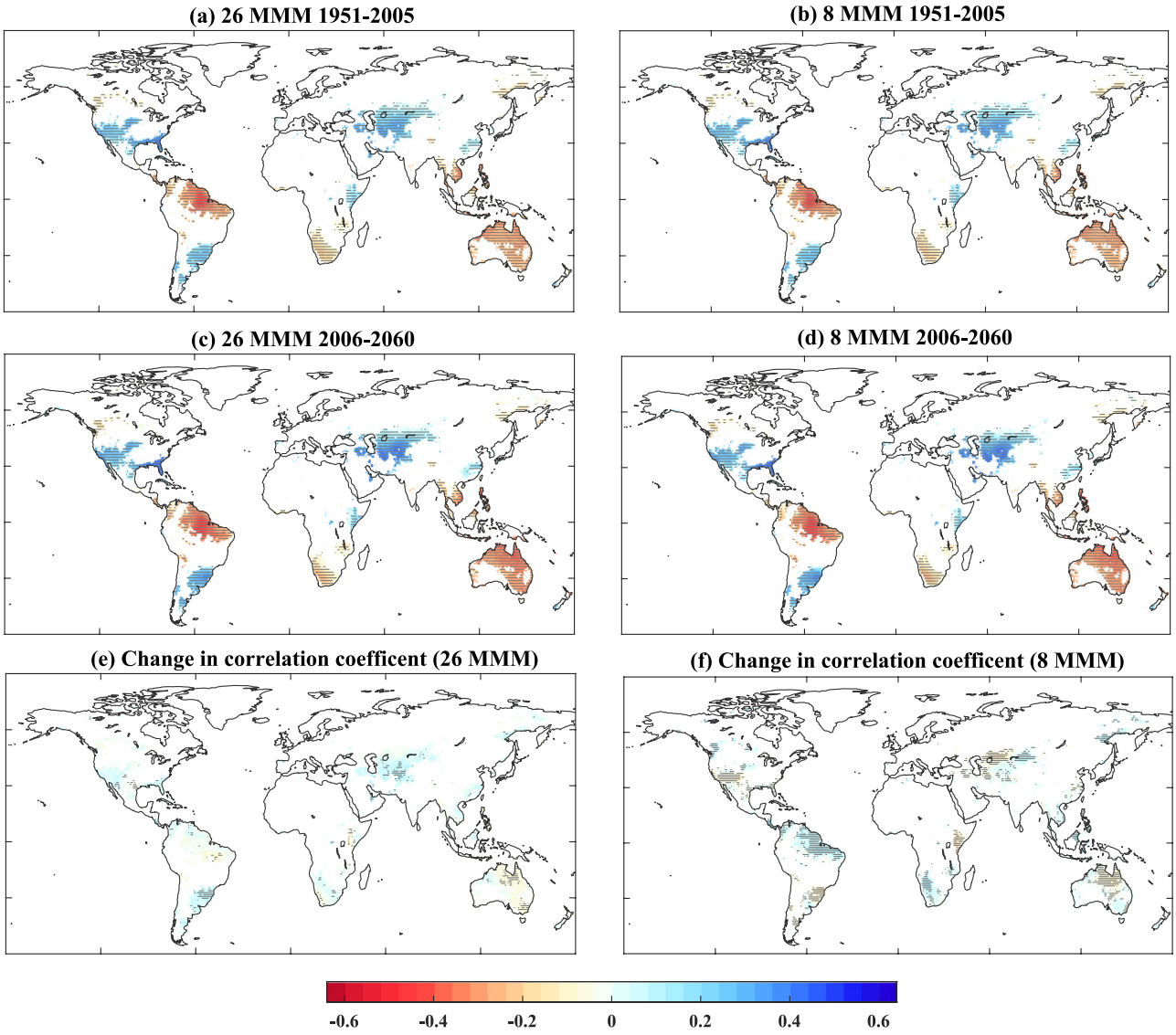

FIG. 3. Correlation coefficients for the relationship between the normalized ONI value and the SPI values during the period 1951–2005, for (a),(c),(e) the MMM of all 26 models and (b),(d),(f) the MMM of the 8 selected models. (a),(b) The MMM of the historical simulations (1951–2005); (c),(d) the MMM of the RCP4.5 simulations (2006–60); (e),(f) changes in the correlation coefficient between the historical simulations and the RCP4.5 simulations. Stippling denotes locations for which at least two-thirds of the models agree with the sign of the MMM results.

patterns over southwestern North America, southern China, and central Asia during La Niña phases but wetter patterns over northeastern South America, Australia, and southern Africa during La Niña phases. Moreover, we compared precipitation anomalies under different ENSO events for the two subperiods 1951–80 and 1981–2010 (Fig. ES5). We removed the influence of the Pacific decadal oscillation (PDO) from the observations by linear regression. Then, we compared the composite patterns of the La Niña and El Niño phases during the 1951–80 and 1981–2010 periods over the grid cells with a significant relationship between ENSO and SPI. The results show that ENSO-related precipitation anomalies in the period 1981–2010 were larger than those in the period 1951–80 for the northeast and southeast of South America and for some regions scattered in southwest Asia (Fig. ES5), but the differences were not significant according to the Mann–Whitney *U* test.

Compared with the results from single model (Fig. 2, Figs. ES6 and ES7), the MMMs of the 26 models and of the 8 selected models were able to capture the observed teleconnection patterns (Figs. 3a,b). The sign of the anomalous precipitation over global land as captured by the MMMs

of all 26 models and of the 8 selected models (Figs. ES3 and ES4) was in agreement with that produced individually by two-thirds or more of the models used. The spatial correlation coefficients between the model composite SPI patterns and the observed composite SPI patterns in response to La Niña and El Niño were higher in the ensemble mean than in the individual models (Fig. 2). This is consistent with the evaluation of ENSO precipitation teleconnections described elsewhere (Power and Delage 2018). This may be because the multimodel ensemble embraces distinctly different physical parameterizations, thus surmounting the limitations of an overconfident single-model simulation (Tebaldi and Knutti 2007).

Changes in precipitation response patterns. **Gridcell scale.** Overall, the geographical area with a significant relationship between the ENSO index and SPI values under the RCP4.5 scenario broadly resembled what we found for the observed data and simulated historical periods (Figs. 3c,d). According to the MMM of the 26 models, the correlation coefficients are projected to increase in the future (Fig. 3e), relative to the historical period, in southern North America, southern South America, southwestern central Asia, Australia, and in some grids scattered in southeastern China. Precipitation variability in these regions has been shown to be connected to ENSO variation (Ropelewski and Halpert 1986, 1987; Mariotti 2007; Grimm and Tedeschi 2009; Juneng and Tangang 2005). However, the MMM of the 8 selected models did not show this consistent strengthening of the relationship between the ENSO index values and SPI value in some of these regions. The consistent strengthening can be found across both the 26 models and the 8-model subset only in northern Australia and parts of central Asia.

Under the RCP4.5 scenario, some regions of southern North America, southern South America, and southern central Asia were predicted to experience drier conditions (higher negative anomalous precipitation) during La Niña phases, while wetter conditions were predicted for Southeast Asia and Australia in both the MMM of the 26 models (Fig. 4a) and the MMM of the 8 selected models (Fig. 4c). Two-thirds or more of the models used agreed as to

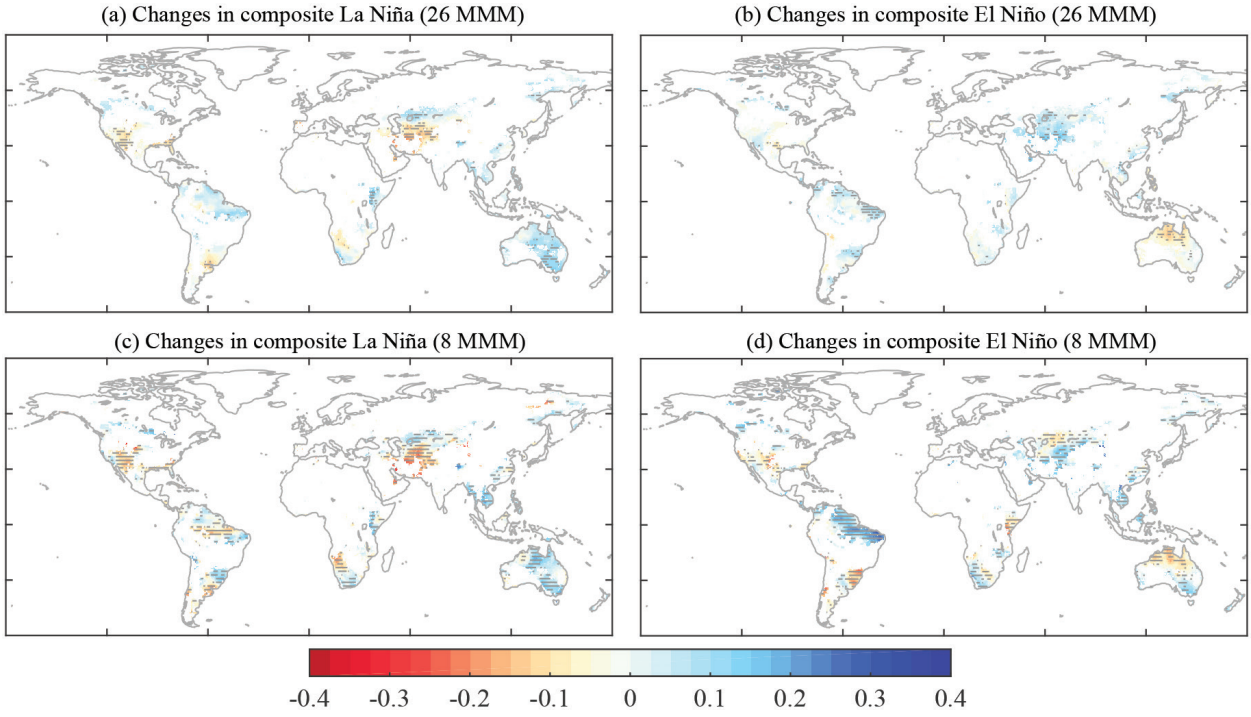

Fig. 4. Changes in the composite of the annual SPI values in response to strong ENSO events for the RCP4.5 simulations (2006–60) relative to the historical simulations (1951–2005). (a),(b) The MMM of the 26 models; (c),(d) the MMM of the 8 selected models. Stippling indicates regions where the sign of the MMM change is the same as the sign in at least two-thirds of the models used.

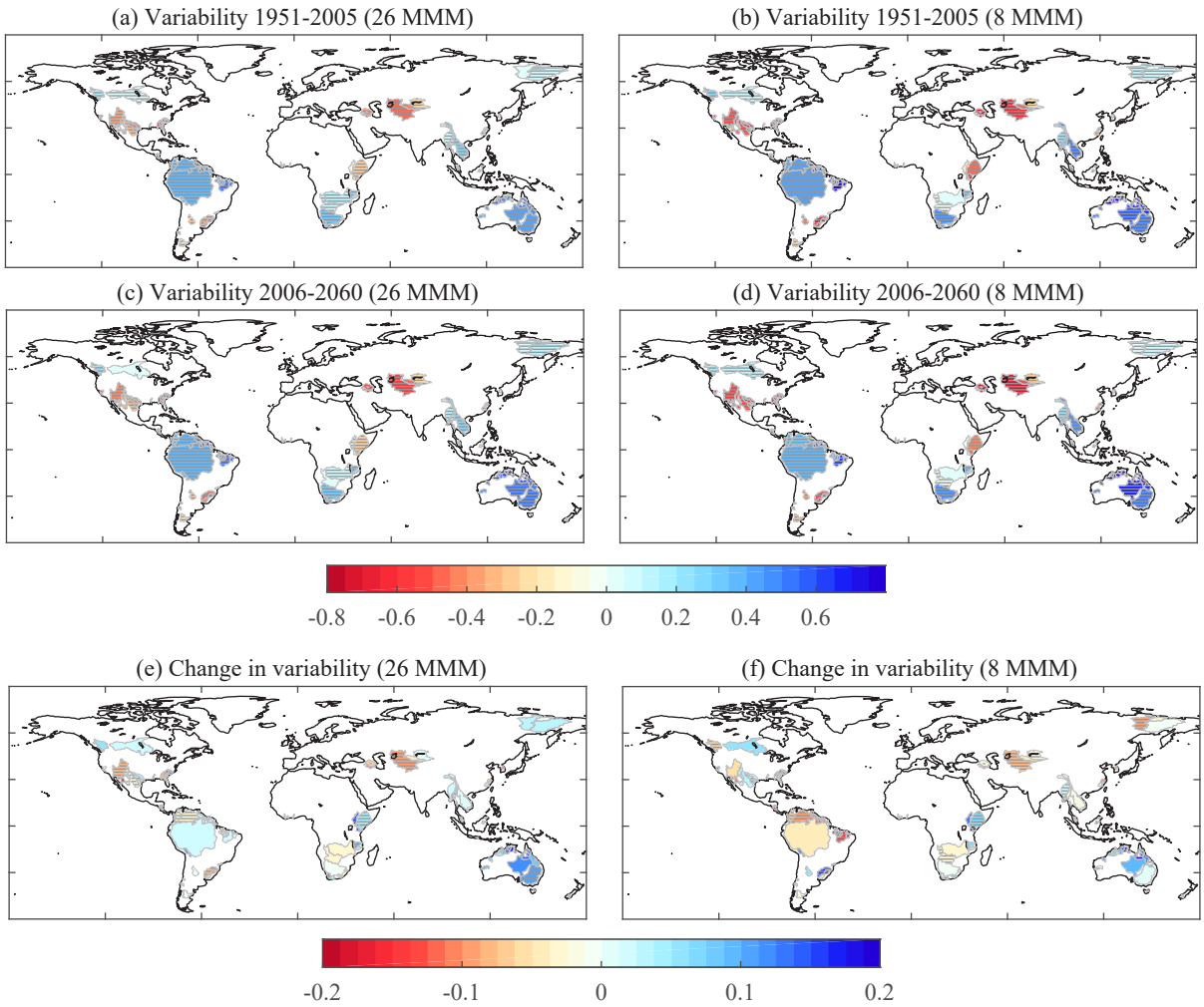

Fig. 5. ENSO-related precipitation variability for 117 river basins based on the MMMs of the 26 models and the 8 selected models. (a),(b) ENSO-related precipitation variability (composite SPI values for La Niña years minus composite SPI values for El Niño years) for the MMM of the historical period (1951–2005); (c),(d) ENSO-related precipitation variability for RCP4.5 (2006–60) simulations. (e),(f) ENSO-related precipitation variability for the RCP4.5 scenario minus ENSO-related precipitation variability for the historical simulations. Stippling in (a)–(f) indicates regions where at least two-thirds of models used agree with the sign in the MMM.

the signs of these changes. However, there was little obvious strengthening of anomalous precipitation during El Niño phases, except in southern central Asia and northern Australia. Some regions were predicted to experience a slight weakening of anomalous precipitation during El Niño phases, such as Southeast Asia and South America (Figs. 4b,d). The results from the 26 models and the best 8 selected models showed a closer transition pattern during La Niña phases than that during El Niño phases. The spatial correlation coefficients between the MMMs of the 26 models and the 8 selected models are 0.73 and 0.47 for the transition patterns during La Niña phases and El Niño phases, respectively. Precipitation anomalies in South America, southwestern North America, and northern central Asia during El Niño phases had inconsistent change signals.

River-basin scale. Figures 5 and 6 showed the changes in regional precipitation response patterns to future ENSO events at the river-basin scale. Once more, the MMM performed better than the individual models when simulating the teleconnections between regional precipitation variability and ENSO, with a correlation coefficient greater than 0.8 (0.8) for the La Niña (El Niño) composite pattern (Fig. 2b). The time series of the regional average SPI

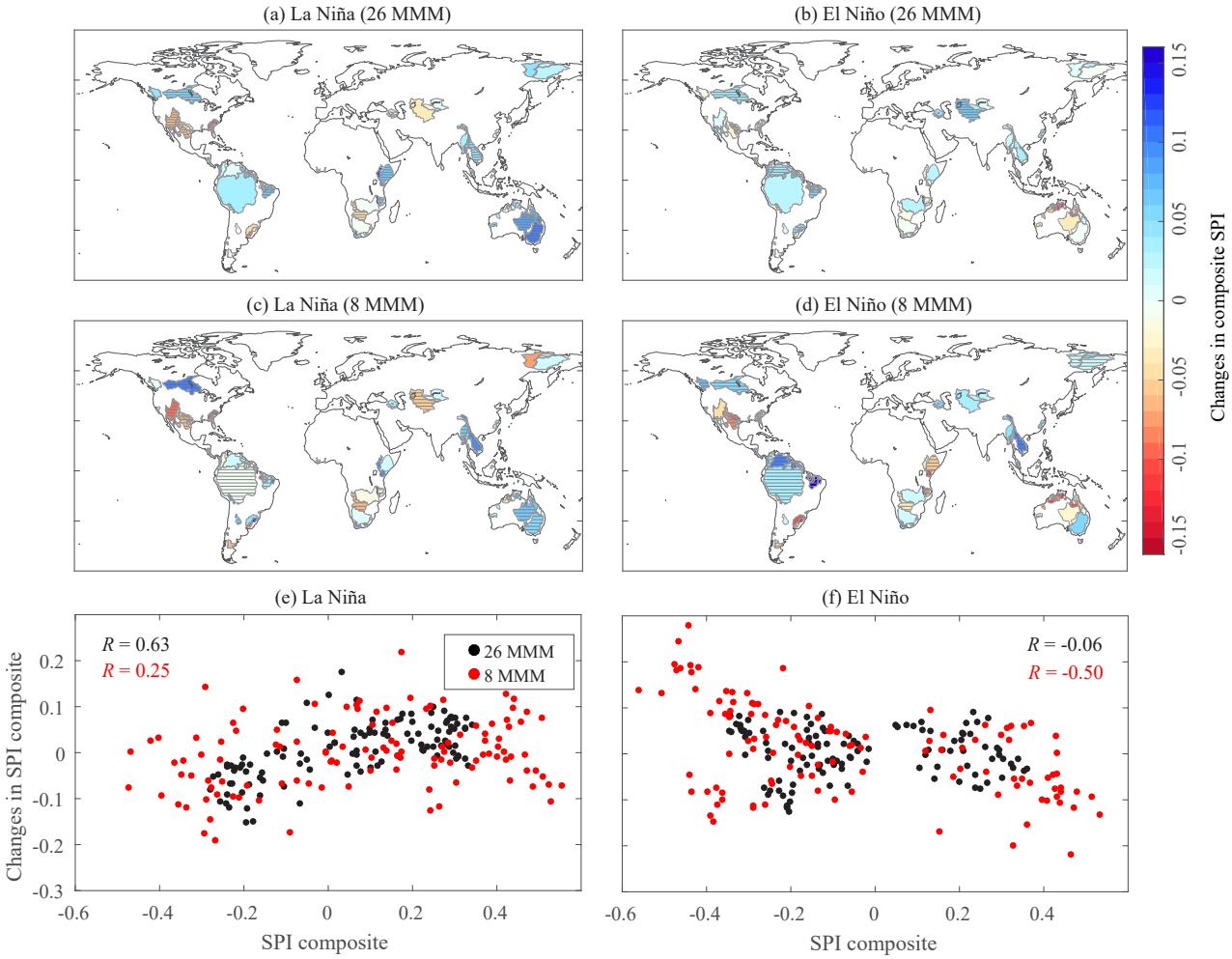

FIG. 6. Projected changes in the regional SPI values during strong La Niña and El Niño phases in 117 major river basins. (a),(c) Maps of the changes in the regional SPI composite over 117 major river basins for strong La Niña events based, respectively, on the MMMs of all 26 models and the 8 selected models. (b),(d) Maps for El Niño phases. Stippling in (a)–(d) indicates regions where the signal of the change in the MMM is the same as the signal in two-thirds or more of the models used. (e),(f) The relationship between the historical regional SPI composite and changes in the regional SPI composite over 117 major river basins, for strong La Niña and El Niño phases, respectively. The black and red dots indicate the results from the MMMs of all 26 models and the 8 selected models, respectively.

values were calculated, and then the regional average composite SPI was derived to estimate the response of precipitation to ENSO. We quantified changes in ENSO-related precipitation variability by comparing the historical and projected differences between the composite SPI values in response to La Niña and El Niño phases (Fig. 5). ENSO-driven precipitation variability was projected to increase slightly in river basins over southwestern North America, the Murray River basin, and the Aral basin based on the MMMs of the 26 models and the 8 selected models. However, these MMMs showed different change signals for precipitation variability in the river basins of South America. The predicted future precipitation response to La Niña and El Niño was asymmetric. Under the RCP4.5 scenario, a "dry to drier, wet to wetter" pattern during La Niña phases was projected in some river basins, including the river basins of southern North America, central Asia, Southeast Asia, and Australia. The results from the MMMs of the 26 models and the 8 selected models agreed with regard to the signals of these changes. The MMM of the 26 models showed that changes in the regional composite SPI, during La Niña phases were significantly positively correlated with the historical composite SPI with a correlation coefficient of 0.63 (Fig. 6e), while the MMM of the 8

selected models did not show such a strong relationship, due to inconsistent change signals in some river basins (Figs. 6a,c). For example, in the Amazon River basin, the results from the 26 models and the 8 selected models had opposite change signals. During future El Niño phases, the "dry to drier, wet to wetter" pattern was not seen over most river basins. To the contrary, the historical negative precipitation anomalies over the Amazon River and Mekong River basins and the positive anomalies over the river basins of northern North America were projected to be ameliorated. Generally speaking, there are large uncertainties in the changes of precipitation anomalies during future El Niño phases, with large inconsistences evident between the MMMs of the 26 models and the 8 selected models.

Changes in the occurrence of severe dry/wet events. Figures 7 and 8 showed changes in the frequency of severe dry/wet events under future ENSO conditions over 117 river basins. Assessment of these basins revealed large geographical differences in the projected changes in the frequency of severe dry and wet events. Under RCP4.5, according to both the MMMs of the 26 models and the 8 selected models, 45 rivers under El Niño conditions and 39 river basins under La Niña conditions were predicted to experience an increase in the frequency of severe dry events relative to the historical period, while 44 under El Niño conditions and 44 under La Niña conditions would experience decreasing trends. Conversely, 59 river basins under El Niño conditions and 61 under La Niña conditions were predicted to have an increase in the frequency of severe wet events, suggesting a likely increase in the risk of floods, while a decreasing tendency was found for 21 river basins under El Niño conditions and 17 under La Niña conditions. Both intense dry events and excessive flooding were projected to increase in frequency in 22 river basins during La Niña phases, including the Aral River basin, the Colorado River basin, and the southern river basins of North America, indicating that these

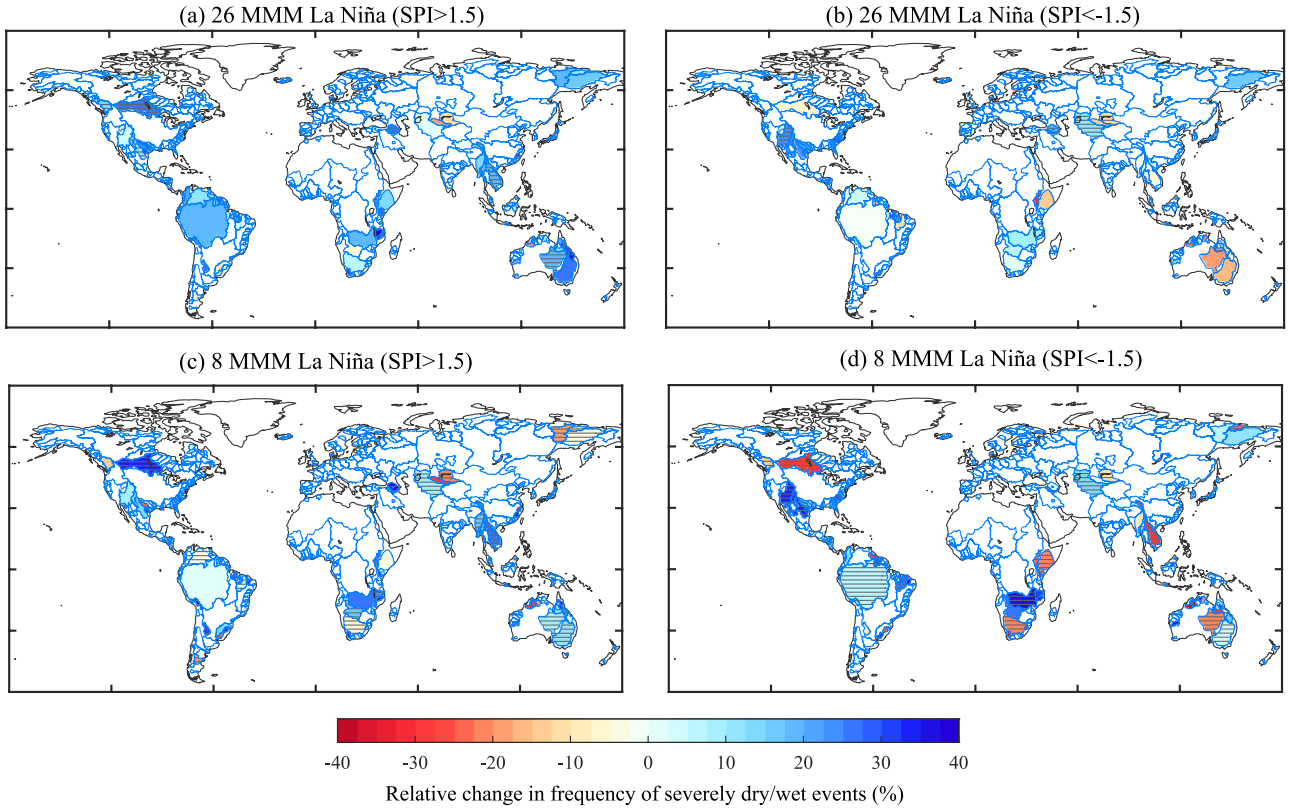

Fig. 7. Projected relative changes in the frequency of severe dry events (SPI < –1.5) and severe wet events (SPI > 1.5) during strong La Niña phases in 117 major river basins. The analysis is based on the MMM change (a),(b) for the 26 models and(c),(d) for the 8 selected best models. Stippling in the panels indicates that the sign of the change in the multimodel ensemble is the same as the sign in two-thirds or more of the models used.

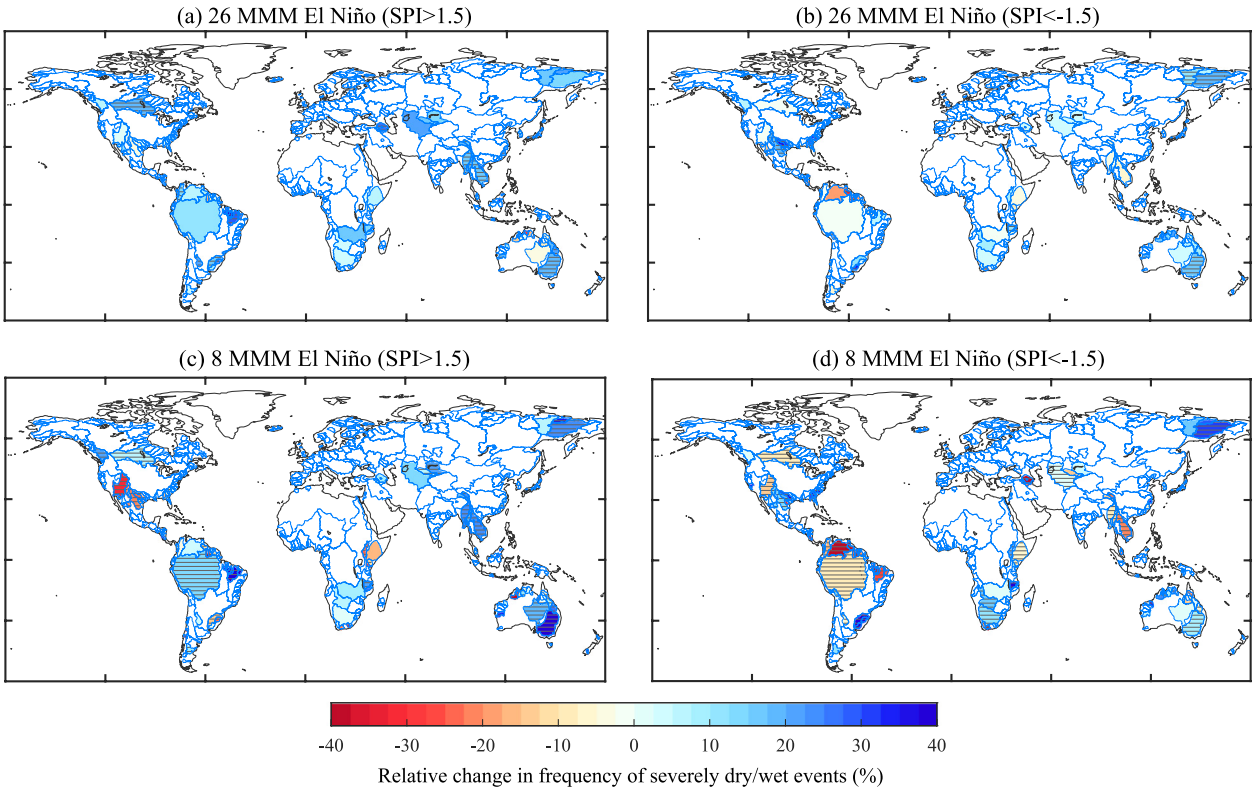

FIG. 8. Projected relative changes in the frequency of severe dry events (SPI < –1.5) and severe wet events (SPI > 1.5) during strong El Niño phases in 117 major river basins. The analysis is based on the MMM change (a),(b) for the 26 models and (c),(d) for the 8 selected best models. Stippling in the panels indicates that the sign of the change in the multimodel ensemble is the same as the sign in two-thirds or more of the models used. The blue lines indicate the boundaries of the major river basins.

rivers may experience concurrent dry condition and wet condition in different parts of their basins during ENSO events. Some basins, such as the Mekong River basin, the Murray River basin, and river basins in Canada, were predicted to experience an increase in the frequency of severe wet events but a decrease in the frequency of dry events during La Niña phases (Fig. 7). Most river basins showed a broad increase in the frequency of severe wet events during El Niño phases. The Murray River basin and the Mekong River basin showed more pronounced and robust changes, with agreement from more than two-thirds of the models (Figs. 8a,c).

Figure 9 exhibited the relationship between the change in regional composite SPI and the change in the frequency of dry/wet events over different river basins. The correlation coefficients based on the simulations from all 26 models and the 8 selected models indicate that the changes in the frequency of severe dry/wet events contributed to the changes in anomalous precipitation in response to ENSO events. We also examined the relationship between the change in the frequency of severe events and historical anomalous precipitation. The significant negative correlation coefficient indicates that the river basins with large negative anomalous precipitation are predicted to experience an increase in severe dry events during La Niña.

However, a decrease in the total number of dry/wet events in a full year and a reduction in anomalous precipitation do not necessarily indicate a weakening of dry or wet events. For instance, in the Amazon River basin, drought events and below-average streamflow are commonly associated with El Niño events (Lopes et al. 2016); we found a decrease in dry events but an increase in wet events from the MMM of the 26 models under the RCP4.5 scenario, albeit without general agreement among most models. However, looking at the changes in individual months, dry events did not decrease from October to December, when the teleconnection relationship with ENSO is much stronger (Fig. 10a). Moreover, with an increased occurrence of extreme ENSO events, more areas were predicted to be subject to a greater frequency of dry

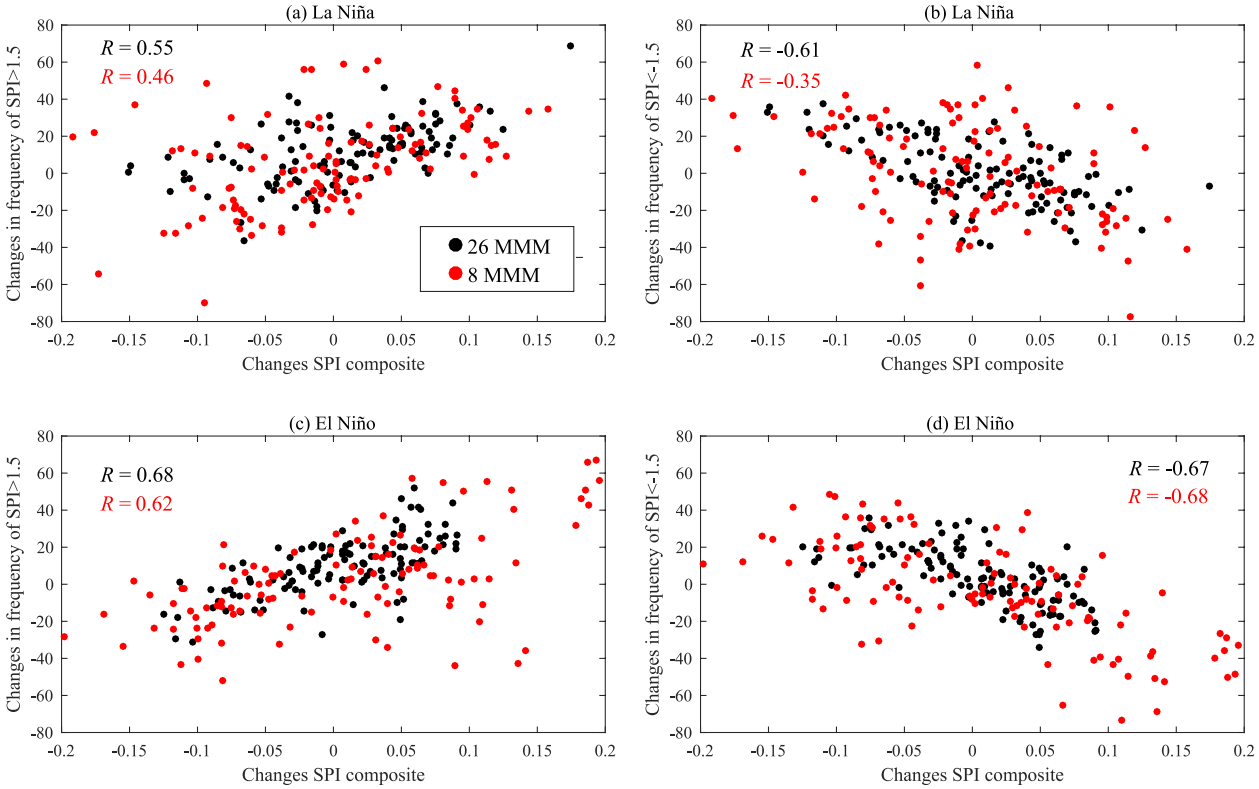

FIG. 9. The relationship between the change in the regional SPI composite values and the change in the frequency of severe dry/wet events during strong (a),(b) La Niña and (c),(d) El Niño phases. The dots indicate 117 major river basins in which the dry/wet conditions are significantly correlated with ENSO. The black and red dots indicate the results from the MMMs of the 26 models and the 8 selected models, respectively.

events and floods. For instance, with an ENSO-index threshold of two standard deviations, the risk of dry events during El Niño phases and floods during La Niña phases was predicted to increase in the Amazon River basin. In the Colorado River basin, dry event was predicted to be more frequent and widespread under RCP4.5 in response to increasingly strong La Niña events (Fig. 11).

Discussion and conclusions

In summary, anomalous precipitation under different ENSO conditions may be changed in some regions under future climate warming, with an asymmetric response to La Niña and El Niño. We analyzed precipitation response patterns to La Niña and El Niño phases and found that a "dry to drier, wet to wetter" annual anomalous precipitation pattern was predicted for La Niña phases, with drier conditions expected over southern North America, southern South America, and southern central Asia, and wetter conditions expected in Southeast Asia and Australia based on analysis of results from all 26 models and the 8 selected models with good performance. However, a similar strengthening of anomalous precipitation was not observed for El Niño phases and, in fact, a slight weakening of annual anomalous precipitation was predicted for Southeast Asia and South America during El Niño phases. The future changes in anomalous precipitation during La Niña phases is more robust than that during El Niño phases, according to the comparison of the results from the 26 models and the 8 selected models. The asymmetric response of anomalous precipitation to La Niña and El Niño suggests that the influences of ENSO on precipitation may change in the future, but the existing teleconnections will probably not simply be strengthened and remain uncertainties. Further exploration of the underlying mechanisms that contribute to these changes in teleconnection relationships remains an avenue for future work. On the other hand, our study mainly

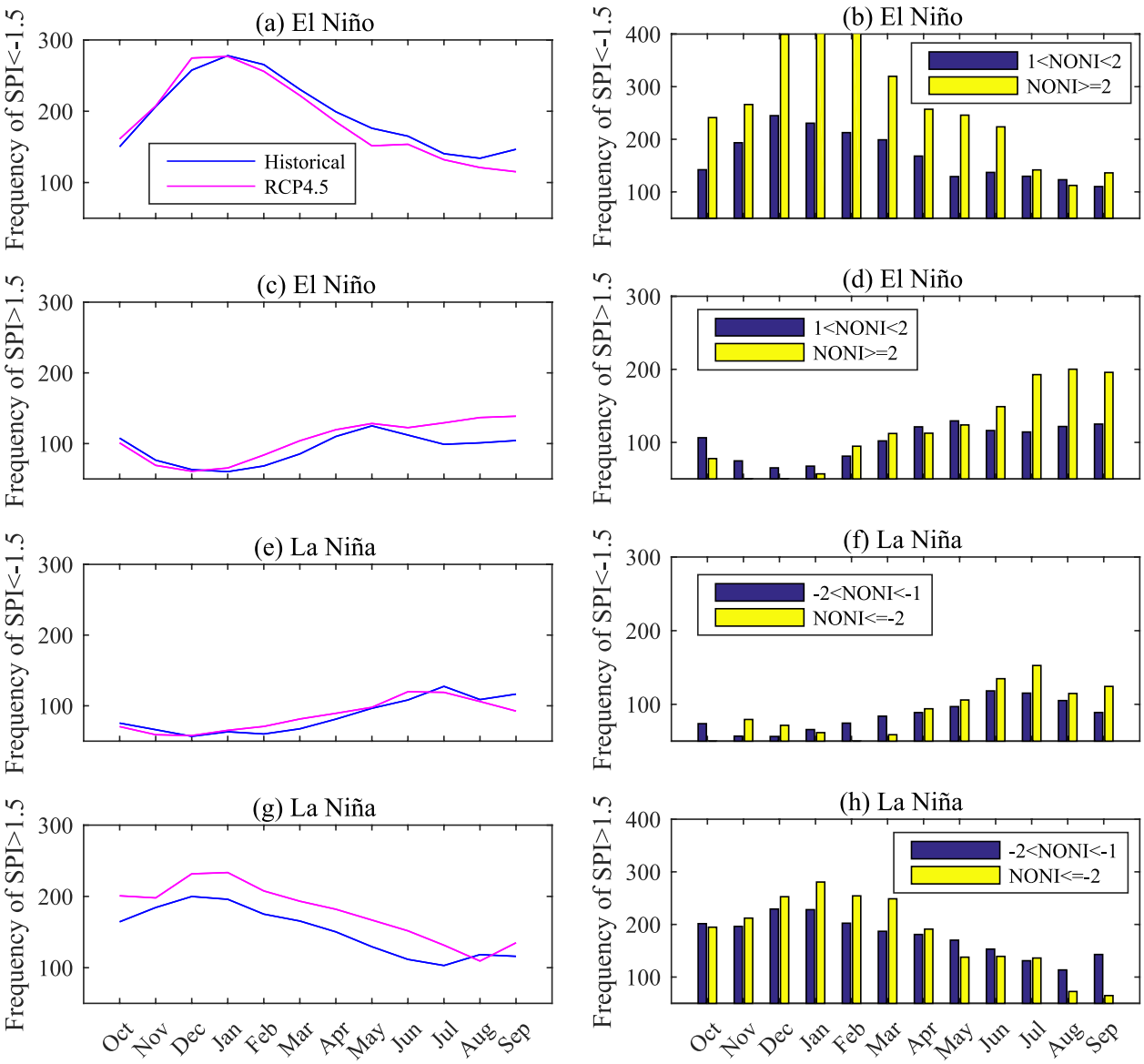

FIG. 10. The average frequency of dry/wet events of different intensities over the Amazon River basin during (a)–(d) strong El Niño years and (e)–(h) strong La Niña years. (a),(c),(e),(g) The average number of dry/wet events is measured as the number of months in which the detrended monthly SPI value exceeded specified thresholds (SPI < –1.5 for severe dry events; SPI > 1.5 for severe wet events). The blue and magenta lines indicate the results from historical and RCP4.5 simulations, respectively.

focused on changes in the ENSO driven precipitation variability. Power and Delage (2018) also revealed changes in mean state and neutral precipitation over the globe, which may modify the ENSO teleconnections to some extent. Quantification and explanation for the contribution of mean state changes to changes in ENSO teleconnections is an important topic for future climatic conditions.

With these changes in precipitation anomalies in response to future ENSO events, the majority of river basins were predicted to experience an increase in the frequency of ENSO-related severe dry/wet events. For instance, precipitation deficits in El Niño years over the ENSO-affected Australia region were predicted to worsen and, in combination with higher temperatures under a warmer climate, may trigger more extreme droughts. Central Asia has a semiarid steppe climate with little precipitation, and precipitation variability there can be affected by variations in ENSO (Mariotti 2007). Furthermore, much of the population in this region is directly reliant on agriculture. This region may become more susceptible to droughts in La Niña years owing to intensified negative SPI anomalies and an increased

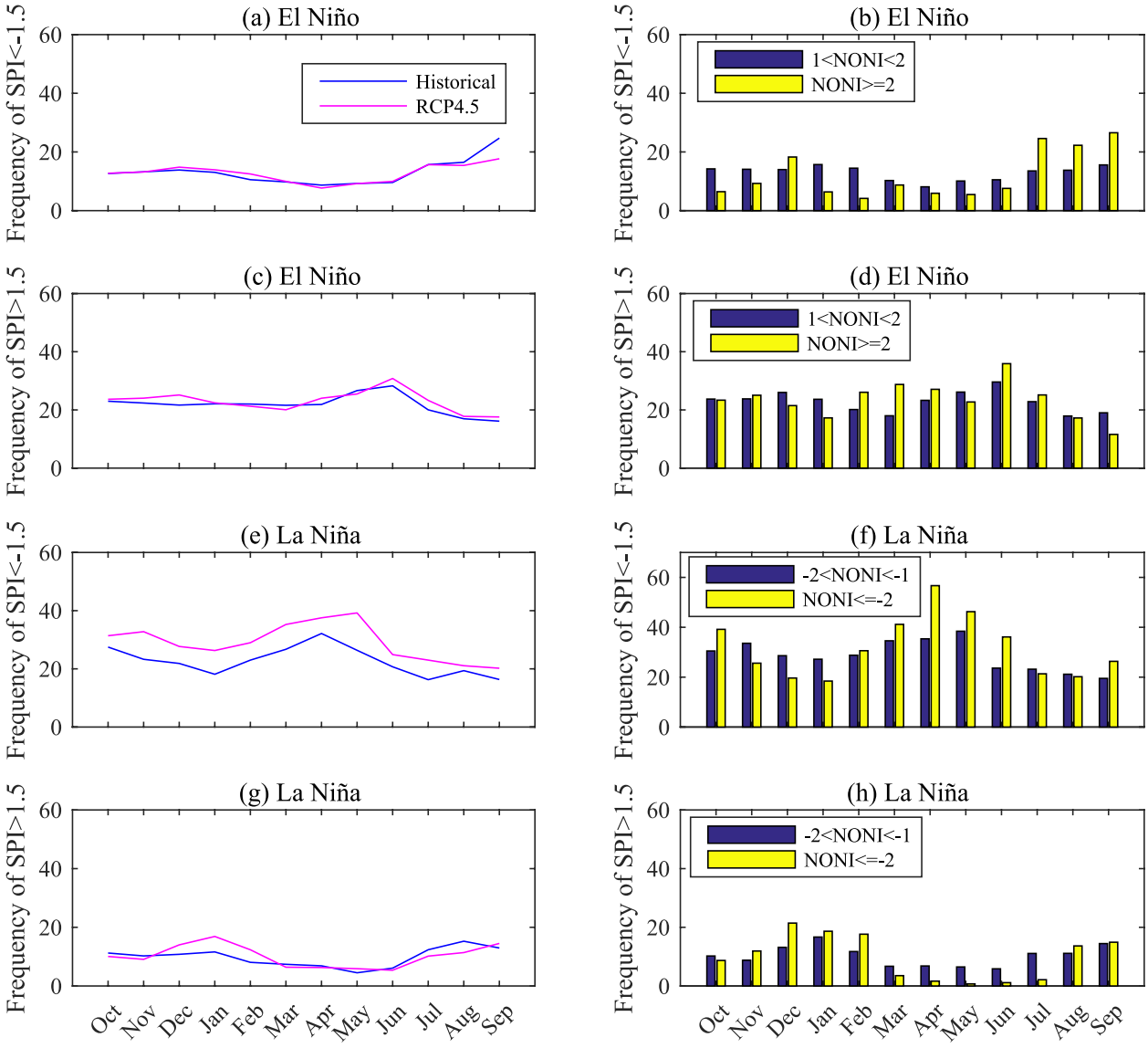

Fig. 11. The average frequency of dry/wet events of different intensities over the Colorado River basin during (a)–(d) strong El Niño years and (e)–(h) strong La Niña years. (a),(c),(e),(g) The average number of dry/wet events is measured as the number of months in which the detrended monthly SPI value exceeded specified thresholds (SPI < –1.5 for severe dry events; SPI > 1.5 for severe wet events). The blue and magenta lines indicate the results from historical and RCP4.5 simulations, respectively.

frequency of dry events. A shortage of water resources in this region would pose a great threat to agriculture and human health and would likely trigger regional conflicts. With the strengthening of negative anomalous precipitation and a predicted increase in the frequency of extreme La Niña events, the Colorado River basin may be subjected to a greater frequency of dry events, which in turn may affect water supply in the southwestern United States (e.g., in California). The changes of ENSO teleconnections and the increasing frequency of ENSO-related extreme events suggest that it is essential to take projected changes in ENSO characteristics and teleconnections into consideration when improving seasonal or long-term drought and flood predictions. In contrast to concurrent climate extremes, such as simultaneous droughts and heat waves (AghaKouchak et al. 2014), successive extreme events caused by shifts in the ENSO cycle would result in an inverse hazard map and severe compound effects, increasing the temporal imbalance of water availability and posing new challenges for the management of freshwater resources and engineering facilities. New multihazard-resilient criteria for infrastructure design will be needed to cope with the

projected changes in the ENSO cycle, and consequently with the changes in ENSO-driven extreme events (Yeh et al. 2018).

The projected changes in ENSO influences may be related to several potential factors. First, changes in the properties and features of ENSO events, such as an increase in high-magnitude ENSO events, can affect anomalies in dry/wet patterns and extreme weather events over global land. The combination of changes in the features of ENSO events with an overall warming climatic state may perturb large circulation patterns, with subsequent effects on weather events over land. Power et al. (2013) suggested that anomalous convection will be greater in the twenty-first century than the twentieth century because of background warming in the equatorial Pacific; with changes in ENSO variance and structural changes in ENSO sea surface temperature anomalies, the nonlinear contribution of background warming to intensified precipitation may be enhanced or dampened. On the other hand, precipitation anomalies would be expected to increase under a warming climate even if there were no changes in ENSO properties: a warmer atmosphere tends to hold more moisture, resulting in a greater frequency of extreme rainfall events with higher rainfall intensity (Trenberth 2011). Although we detrended the time series, used a traditional composite method, and considered whether there was robust agreement from multiple models in our study of ENSO-related effects on variability in global land precipitation, precipitation anomalies may also be modified by other thermodynamic and dynamic processes. Some studies have pointed out that an increase in the frequency of dry events and an increase in the intensity of the most extreme events can result in increases in the interannual variability of the annual hydroclimate. For instance, Polade et al. (2014, 2017) and Swain et al. (2018) predicted that, owing to the combined effects of dynamically strengthened onshore vapor transport and the thermodynamic enhancement of vapor transport, the frequency of dry days and extreme events will increase over the southwestern United States, especially in California, leading to increased sampling variability of the annual hydroclimate (Polade et al. 2017; Swain et al. 2018).

However, changes in ENSO itself and in the related remote influences on precipitation variability over global land are controversial and accompanied by a large degree of uncertainty. Although the ability of CMIP5 models to simulate ENSO has improved compared with previous versions (Bellenger et al. 2014), there are still substantial intermodel differences in the changes in the projected spatial structure and amplitude of ENSO (Watanabe et al. 2012) and future ENSO-driven teleconnections, especially in the changes to projected precipitation anomalies during future El Niño phases. On the other hand, quantifying the teleconnection influence of ENSO on climate is subject to uncertainty owing to aliasing of unrelated climate variability, even with nearly a century of observations, which inevitably poses challenges for the evaluation of ENSO teleconnections in models and the projection of future changes in these teleconnections (Deser et al. 2017, 2018). Further studies to identify model biases in how they respond to ENSO simulated from historical climate forcing and apparent model biases that arise from limited sampling of internal variability unrelated to ENSO are essential and should use longer observational records and large model ensembles.

Acknowledgments. Funding for this research was provided by the National Natural Science Foundation of China (41622101 and 41877155), the National Key Research and Development Program of China (2016YFC0501604), the State Key Laboratory of Earth Surface Processes and Resource Ecology, and the Fundamental Research Funds for the Central Universities. We acknowledge the World Climate Research Programme's Working Group on Coupled Modelling, which is responsible for CMIP, and we thank the climate modeling groups (listed in Table ES1 of this paper) for producing and making available their model outputs. We are also grateful to the Global Precipitation Climatology Centre (GPCC) for providing the observed precipitation data, and to the Climate Prediction Center (CPC) for providing the climate signals from the oceans.

References

AghaKouchak, A., L. Cheng, O. Mazdiyasni, and A. Farahmand, 2014: Global warming and changes in risk of concurrent climate extremes: Insights from the 2014 California drought. *Geophys. Res. Lett.*, **41**, 8847–8852, https://doi.org/10.1002/2014GL062308.

Alexander, M. A., I. Bladé, M. Newman, J. R. Lanzante, N. C. Lau, and J. D. Scott, 2002: The atmospheric bridge: The influence of ENSO teleconnections on air–sea interaction over the global oceans. *J. Climate*, **15**, 2205–2231, https://doi.org/10.1175/1520-0442(2002)015<2205:TABTIO>2.0.CO;2.

Allen, R. J., and R. Luptowitz, 2017: El Niño-like teleconnection increases California precipitation in response to warming. *Nat. Commun.*, **8**, 16055, https://doi.org/10.1038/ncomms16055.

Andela, N., and G. R. van der Werf, 2014: Recent trends in African fires driven by cropland expansion and El Niño to La Niña transition. *Nat. Climate Change*, **4**, 791–795, https://doi.org/10.1038/nclimate2313.

Barlow, M., H. Cullen, and B. Lyon, 2002: Drought in central and southwest Asia: La Niña, the warm pool, and Indian Ocean precipitation. *J. Climate*, **15**, 697–700, https://doi.org/10.1175/1520-0442(2002)015<0697:DICASA>2.0.CO;2.

Bell, G. D., M. S. Halpert, C. F. Ropelewski, V. E. Kousky, A. V. Douglas, R. C. Schnell, and M. E. Gelman, 1999: Climate assessment for 1998. *Bull. Amer. Meteor. Soc.*, **80**, S1–S48, https://doi.org/10.1175/1520-0477-80.5s.S1.

Bellenger, H., E. Guilyardi, J. Leloup, M. Lengaigne, and J. Vialard, 2014: ENSO representation in climate models: From CMIP3 to CMIP5. *Climate Dyn.*, **42**, 1999–2018, https://doi.org/10.1007/s00382-013-1783-z.

Bonfils, C. J., B. D. Santer, T. J. Phillips, K. Marvel, L. R. Leung, C. Doutriaux, and A. Capotondi, 2015: Relative contributions of mean-state shifts and ENSO-driven variability to precipitation changes in a warming climate. *J. Climate*, **28**, 9997–10013, https://doi.org/10.1175/JCLI-D-15-0341.1.

Brekke, L., A. Wood, and T. Pruitt, 2014: Downscaled CMIP3 and CMIP5 hydrology projections: Release of hydrology projections, comparison with preceding information, and summary of user needs. Tech. Rep., National Center for Atmospheric Research, 111 pp., https://gdo-dcp.ucllnl.org/downscaled_cmip_projections/techmemo/BCSD5HydrologyMemo.pdf.

Cai, W., and Coauthors, 2014: Increasing frequency of extreme El Niño events due to greenhouse warming. *Nat. Climate Change*, **4**, 111–116, https://doi.org/10.1038/nclimate2100.

——, and Coauthors, 2015a: ENSO and greenhouse warming. *Nat. Climate Change*, **5**, 849–859, https://doi.org/10.1038/nclimate2743.

——, and Coauthors, 2015b: Increased frequency of extreme La Niña events under greenhouse warming. *Nat. Climate Change*, **5**, 132–137, https://doi.org/10.1038/nclimate2492.

Chand, S. S., K. J. Tory, H. Ye, and K. J. E. Walsh, 2017: Projected increase in El Niño-driven tropical cyclone frequency in the Pacific. *Nat. Climate Change*, **7**, 123–127, https://doi.org/10.1038/nclimate3181.

Coelho, C. A. S., and L. Goddard, 2009: El Niño–induced tropical droughts in climate change projections. *J. Climate*, **22**, 6456–6476, https://doi.org/10.1175/2009JCLI3185.1.

Deser, C., I. R. Simpson, K. A. McKinnon, and A. S. Phillips, 2017: The Northern Hemisphere extra-tropical atmospheric circulation response to ENSO: How well do we know it and how do we evaluate models accordingly? *J. Climate*, **30**, 5059–5082, https://doi.org/10.1175/JCLI-D-16-0844.1.

——, ——, A. S. Phillips, and K. A. McKinnon, 2018: How well do we know ENSO's climate impacts over North America, and how do we evaluate models accordingly? *J. Climate*, **31**, 4991–5014, https://doi.org/10.1175/JCLI-D-17-0783.1.

Donat, M. G., A. L. Lowry, L. V. Alexander, P. A. O'Gorman, and N. Maher, 2017: More extreme precipitation in the world's dry and wet regions. *Nat. Climate Change*, **7**, 154–158, https://doi.org/10.1038/nclimate3160.

Grimm, A. M., and R. G. Tedeschi, 2009: ENSO and extreme rainfall events in South America. *J. Climate*, **22**, 1589–1609, https://doi.org/10.1175/2008JCLI2429.1.

Hirabayashi, H., R. Mahendran, S. Koirala, L. Konoshima, D. Yamazaki, S. Watanabe, H. Kim, and S. Kanae, 2013: Global flood risk under climate change. *Nat. Climate Change*, **3**, 816–821, https://doi.org/10.1038/nclimate1911.

Hoerling, M., and A. Kumar, 2003: The perfect ocean for drought. *Science*, **299**, 691–694, https://doi.org/10.1126/science.1079053.

Iizumi, T., J. J. Luo, A. J. Challinor, G. Sakurai, M. Yokozawa, H. Sakuma, M. E. Brown, and T. Yamagata, 2014: Impacts of El Niño Southern Oscillation on the global yields of major crops. *Nat. Commun.*, **5**, 3712, https://doi.org/10.1038/ncomms4712.

Juneng, L., and F. T. Tangang, 2005: Evolution of ENSO-related rainfall anomalies in Southeast Asia region and its relationship with atmosphere-ocean variations in Indo-Pacific sector. *Climate Dyn.*, **25**, 337–350, https://doi.org/10.1007/s00382-005-0031-6.

Kenyon, J., and G. C. Hegerl, 2008: Influence of modes of climate variability on global temperature extremes. *J. Climate*, **21**, 3872–3889, https://doi.org/10.1175/2008JCLI2125.1.

——, and ——, 2010: Influence of modes of climate variability on global precipitation extremes. *J. Climate*, **23**, 6248–6262, https://doi.org/10.1175/2010JCLI3617.1.

King, D., D. J. Karoly, and G. J. van Oldenborgh, 2016: Climate change and El Niño increase likelihood of Indonesian heat and drought. *Bull. Amer. Meteor. Soc.*, **97**, S113–S117, https://doi.org/10.1175/BAMS-D-16-0164.1.

Kug, J., S. An, Y. Ham, and I. Kang, 2010: Changes in El Niño and La Niña teleconnections over North Pacific–America in the global warming simulations. *Theor. Appl. Climatol.*, **100**, 275–282, https://doi.org/10.1007/s00704-009-0183-0.

Lopes, A. V., J. C. H. Chiang, S. A. Thompson, and J. A. Dracup, 2016: Trend and uncertainty in spatial-temporal patterns of hydrological droughts in the Amazon basin. *Geophys. Res. Lett.*, **43**, 3307–3316, https://doi.org/10.1002/2016GL067738.

Mariotti, A., 2007: How ENSO impacts precipitation in southwest central Asia. *Geophys. Res. Lett.*, **34**, L16706, https://doi.org/10.1029/2007GL030078.

Maurer, E. P., and Coauthors, 2014: An enhanced archive facilitating climate impacts and adaptation analysis. *Bull. Amer. Meteor. Soc.*, **95**, 1011–1019, https://doi.org/10.1175/BAMS-D-13-00126.1.

Meehl, G. A., C. Tebaldi, H. Teng, and T. C. Peterson, 2007: Current and future US weather extremes and El Niño. *Geophys. Res. Lett.*, **34**, L20704, https://doi.org/10.1029/2007GL031027.

Neelin, J. D., D. S. Battisti, A. C. Hirst, F. Jin, Y. Wakata, T. Yamagata, and S. E. Zebiak, 1998: ENSO theory. *J. Geophys. Res.*, **103**, 14261–14290, https://doi.org/10.1029/97JC03424.

Ning, L., E. E. Riddle, and R. S. Bradley, 2015: Projected changes in climate extremes over the northeastern United States. *J. Climate*, **28**, 3289–3310, https://doi.org/10.1175/JCLI-D-14-00150.1.

O'Gorman, P. A., and T. Schneider, 2009: The physical basis for increases in precipitation extremes in simulations of 21st-century climate change. *Proc. Natl. Acad. Sci. USA*, **106**, 14773–14777, https://doi.org/10.1073/pnas.0907610106.

Perry, S. J., S. McGregor, A. Sen Gupta, and M. H. England, 2017: Future changes to El Niño-Southern Oscillation temperature and precipitation teleconnections. *Geophys. Res. Lett.*, **44**, 10608–10616, https://doi.org/10.1002/2017GL074509.

Pfahl, S., P. A. O'Gorman, and E. M. Fischer, 2017: Understanding the regional pattern of projected future changes in extreme precipitation. *Nat. Climate Change*, **7**, 423–427, https://doi.org/10.1038/nclimate3287.

Polade, S. D., D. W. Pierce, D. R. Cayan, A. Gershunov, and M. D. Dettinger, 2014: The key role of dry days in changing regional climate and precipitation regimes. *Sci. Rep.*, **4**, 4364, https://doi.org/10.1038/srep04364.

——, A. Gershunov, D. R. Cayan, M. D. Dettinger, and D. W. Pierce, 2017: Precipitation in a warming world: Assessing projected hydro-climate changes in California and other Mediterranean climate regions. *Sci. Rep.*, **7**, 10783, https://doi.org/10.1038/s41598-017-11285-y.

Power, S. B., and J. Callaghan, 2016: Variability in severe coastal flooding, associated storms, and death tolls in southeastern Australia since the mid-nineteenth century. *J. Appl. Meteor. Climatol.*, **55**, 1139–1149, https://doi.org/10.1175/JAMC-D-15-0146.1.

——, and F. P. D. Delage, 2018: The El Niño–Southern Oscillation and associated climatic conditions around the world during the latter half of the twenty-first century. *J. Climate*, **31**, 6189–6207, https://doi.org/10.1175/JCLI-D-18-0138.1.

——, ——, C. Chung, G. Kociuba, and K. Keay, 2013: Robust twenty-first-century projections of El Niño and related precipitation variability. *Nature*, **502**, 541–545, https://doi.org/10.1038/nature12580.

——, ——, ——, H. Ye, and B. Murphy, 2017: Humans have already increased the risk of major disruptions to Pacific rainfall. *Nat. Commun.*, **8**, 14368, https://doi.org/10.1038/ncomms14368.

Richard, Y., S. Trzaska, P. Roucou, and M. Rouault, 2000: Modification of the southern African rainfall variability/ENSO relationship since the late 1960s. *Climate Dyn.*, **16**, 883–895, https://doi.org/10.1007/s003820000086.

Ropelewski, C. F., and M. S. Halpert, 1986: North American Precipitation and temperature patterns associated with the El Niño/Southern Oscillation (ENSO). *Mon. Wea. Rev.*, **114**, 2352–2362, https://doi.org/10.1175/1520-0493(1986)114<2352:NAPATP>2.0.CO;2.

——, and ——, 1987: Global and regional scale precipitation patterns associated with the El Niño/Southern Oscillation. *Mon. Wea. Rev.*, **115**, 1606–1626, https://doi.org/10.1175/1520-0493(1987)115<1606:GARSPP>2.0.CO;2.

Santoso, A., S. McGregor, F. Jin, W. Cai, M. H. England, S. I. An, M. J. McPhaden, and E. Guilyardi, 2013: Late-twentieth-century emergence of the El Niño propagation asymmetry and future projections. *Nature*, **504**, 126–130, https://doi.org/10.1038/nature12683.

Steinhoff, D. F., A. J. Monaghan, and M. P. Clark, 2015: Projected impact of twenty-first century ENSO changes on rainfall over Central America and northwest South America from CMIP5 AOGCMs. *Climate Dyn.*, **44**, 1329–1349, https://doi.org/10.1007/s00382-014-2196-3.

Sun, Q., C. Miao, A. AghaKouchak, and Q. Duan, 2016: Century-scale causal relationships between global dry/wet conditions and the state of the Pacific and Atlantic Oceans. *Geophys. Res. Lett.*, **43**, 6528–6537, https://doi.org/10.1002/2016GL069628.

Swain, D. L., B. Langenbrunner, J. D. Neelin, and A. Hall, 2018: Increasing precipitation volatility in twenty-first-century California. *Nat. Climate Change*, **8**, 427–433, https://doi.org/10.1038/s41558-018-0140-y.

Tebaldi, C., and R. Knutti, 2007: The use of the multi-model ensemble in probabilistic climate projections. *Philos. Trans. Roy. Soc. London*, 365A, 2053–2075, https://doi.org/10.1098/rsta.2007.2076.

Trenberth, K. E., 2011: Changes in precipitation with climate change. *Climate Res.*, **47**, 123–138, https://doi.org/10.3354/cr00953.

Wang, G. M., S. B. Power, and S. McGree, 2016: Unambiguous warming in the western tropical Pacific primarily caused by anthropogenic forcing. *Int. J. Climatol.*, **36**, 933–944, https://doi.org/10.1002/joc.4395.

Wang, S. Y., L. Hipps, R. R. Gillies, and J. H. Yoon, 2014: Probable causes of the abnormal ridge accompanying the 2013–2014 California drought: ENSO precursor and anthropogenic warming footprint. *Geophys. Res. Lett.*, **41**, 3220–3226, https://doi.org/10.1002/2014GL059748.

——, W. R. Huang, H. H. Hsu, and R. R. Gillies, 2015: Role of the strengthened El Niño teleconnection in the May 2015 floods over the southern Great Plains. *Geophys. Res. Lett.*, **42**, 8140–8146, https://doi.org/10.1002/2015GL065211.

Ward, P. J., B. Jongman, M. Kummu, M. D. Dettinger, F. C. S. Weiland, and H. C. Winsemius, 2014: Strong influence of El Niño Southern Oscillation on flood risk around the world. *Proc. Natl. Acad. Sci. USA*, **111**, 15659–15664, https://doi.org/10.1073/pnas.1409822111.

Watanabe, M., J. S. Kug, F. F. Jin, M. Collins, M. Ohba, and A. T. Wittenberg, 2012: Uncertainty in the ENSO amplitude change from the past to the future. *Geophys. Res. Lett.*, **39**, L20703, https://doi.org/10.1029/2012GL053305.

Wood, A. W., L. R. Leung, V. Sridhar, and D. P. Lettenmaier, 2004: Hydrologic implications of dynamical and statistical approaches to downscaling climate model outputs. *Climatic Change*, **62**, 189–216, https://doi.org/10.1023/B:CLIM.0000013685.99609.9e.

Yeh, S. W., and Coauthors, 2018: ENSO atmospheric teleconnections and their response to greenhouse gas forcing. *Rev. Geophys.*, **56**, 185–206, https://doi.org/10.1002/2017RG000568.

Yin, H. F., and C. G. Li, 2001: Human impact on floods and flood disasters on the Yangtze River. *Geomorphology*, **41**, 105–109, https://doi.org/10.1016/S0169-555X(01)00108-8.

Yoon, J. H., S. S. Wang, R. R. Gillies, B. Kravitz, L. Hipps, and P. J. Rasch, 2015: Increasing water cycle extremes in California and in relation to ENSO cycle under global warming. *Nat. Commun.*, **6**, 8657, https://doi.org/10.1038/ncomms9657.

Zhou, Z. Q., S. P. Xie, X. T. Zheng, Q. Y. Liu, and H. Wang, 2014: Global warming-induced changes in El Niño teleconnections over the North Pacific and North America. *J. Climate*, **27**, 9050–9064, https://doi.org/10.1175/JCLI-D-14-00254.1.